Cailleau, B., Oncken, O. (2008): Past forearc deformation in Nicaragua and coupling at the megathrust interface: Evidence for subduction retreat?. - Geochemistry Geophysics Geosystems (G3), 9, Q03016

DOI: 10.1029/2007GC001754.

Past forearc deformation in Nicaragua and coupling at the megathrust interface: Evidence for subduction retreat?

B. Cailleau* and O. Oncken

GFZ Potsdam, Telegrafenberg, D-14473, Germany

* Corresponding author: cailleau@gfz-potsdam.de

Abstract

Deformation at the boundary between the Cocos and Caribbean plates in Nicaragua is currently focused in the volcanic arc in the form of arc-parallel shearing. In the Middle Miocene, however, there was widespread subsidence with local uplift in the outer-forearc and inner-forearc broad uplift. To understand this complex deformation, we use numerical modelling to investigate the effect of inhomogeneous friction at the megathrust fault on strain localisation in the upper plate. A good fit is obtained when 1) the interface between the slab and upper plate is not situated at the current Wadati-Benioff zone but rather is moved 50 km landward to where subduction may have been active in the early Tertiary, and 2) there is high stress accumulation between 15 and 25 km depths and low stress accumulation updip and downdip of the thrust interface. The results are consistent with a high-velocity block being the remnant of an oceanic plateau that subducted in the Eocene and was later incorporated into the upper plate. We suggest that this geometry persisted into the Middle Miocene, before the slab broke off and the thrust interface jumped seaward.

1. Introduction

The present-day Nicaraguan forearc is segmented into various domains with distinct kinematics. To the east, it is bounded by an arc that exhibits shallow

earthquakes with NW-SE dextral shearing at 7 mm/yr along subvertical sinistral arc-normal strike-slip faults (White and Harlow, 1993; La Femina et al., 2002; Cailleau et al., 2007). There is no consensus on the present deformation state of the inner forearc, 80-170 km from the trench. Ranero et al. (2000) suggested that the offshore inner forearc is currently tectonically active. However, the inner forearc does not exhibit any motion and seems to be seismically quiescent (Larsson and Mattson, 1987; Weinberg, 1992) (Fig. 1c). In contrast, the outer forearc, 0-80 km from the trench, shows distributed seismicity and normal faulting associated with uplift (Larsson and Mattson, 1987; Ranero et al., 2000).

Nearly the entire forearc is covered by the 10 km thick Sandino basin, which developed since the late Cretaceous (Weyl, 1980; Ranero et al., 2000) (Figs. 1c and 1d). During the Middle Miocene, parts of this basin were inverted: the eastern margin was uplifted and tilted along NW-trending folds and NE-trending dilatational joints, indicating compression normal to the trench (Weinberg, 1992; Ranero et al., 2000). A portion along the central axis of the basin was also deformed and uplifted (Fig. 1d). This period of partial inversion is associated with a change in sedimentation, from a deep water environment during the early stages to a widespread shallow marine setting (Ranero et al., 2000).

Deeper structures down to 40 km depth have been constrained by seismic wide-angle measurements, gravity, and MT data (Elming and Rasmussen, 1998; Walther et al., 2000) (Fig. 1c). Offshore, the data reveal a high-velocity block (block A in Figure 1c), proposed as the remnant of an oceanic plateau that was subducted and incorporated into the upper plate during the Eocene and Oligocene (Walther et al., 2000). Block B (Fig. 1c) has been interpreted as either the lower crust of the oceanic plateau or dehydrated mantle. The structure of the thrust interface between the subducting slab and

52 the hanging wall was illuminated by the largest historic subduction earthquake in this
53 region, which occurred in 1992 with a magnitude M_s 7.2. The downdip end of the
54 rupture plane was 26 km deep (Ide et al., 1993), which corresponds approximately to
55 the maximum depth of outer forearc seismicity; this indicates a possible relationship
56 between the structure of the megathrust and forearc deformation. During coseismic
57 subduction deformation, a tsunami may have been caused by movement on a splay fault
58 rooting at 10 km depth (Satake, 1994); this would represent the updip limit of the
59 coupling zone, as observed in the Nankai subduction zone (Fukao, 1979; Park et al.,
60 2002).

61 Two scenarios have been proposed for the evolution of the Nicaraguan margin.
62 Ranero et al. (2000) studied shallow structures in the Nicaraguan forearc and favoured a
63 subduction zone active from the Cretaceous to now. Uplift of the outer high and slope
64 by subduction initiation is thought to have acted as a barrier to sediments (Ranero et al.,
65 2000). Widespread subsidence is attributed to basal erosion and local structures to
66 possible transpression along margin-parallel strike-slip faults (Ranero et al., 2000). In
67 contrast, Walther et al. (2000) use seismic wide-angle measurements to suggest a
68 westward migration of subduction or subduction retreat. In their model, the subduction
69 zone was previously located east of the high-velocity block A or plateau, and was active
70 until the Eocene or Oligocene time. The arrival of a buoyant plateau blocked
71 trenchward sediment transport to form the Sandino basin, caused subduction to
72 decelerate and eventually caused the deep slab to detach and be replaced by a mantle
73 sliver (Fig. 1c). The plateau subsequently accreted to the upper plate and a new
74 subduction zone formed west of the plateau.

75

76

Goal of the study

In this study, we seek to understand the enigmatic Middle Miocene phase of upper plate deformation and to reproduce subsidence associated with coastal and local uplift. We also want to constrain the source of forearc deformation and to test whether this deformation can be best explained by westward migration or retreat of subduction. Using finite element modelling, we investigate the relationship between strain localisation in the upper plate and possible frictional heterogeneities along the subduction thrust interface, which has not been previously investigated. We show that upper plate tectonic structures and changes in topography can provide insights into spatial and temporal variations of stress accumulation along the megathrust.

2. Finite Element Method

2a. Physical parameters

We use the finite element program Abaqus (version 6.5). In our 2D models, we focus on deformation of the upper plate in response to downward motion of the slab. The zone of convergence therefore comprises a rigid subducting slab and a deformable overriding plate or hanging wall (Fig. 2). We use a 225 km radius of curvature, which fits the geometry of the present-day slab. The material of the upper plate is elastoplastic with the following characteristics: Young's Modulus is 100 GPa, the density ρ is 2700 kg/m^3, the gravitational constant g is 9.81 m/s^2, Drucker Prager perfect plasticity has a yield stress of 20 MPa (e.g. Fuller et al., 2006; Sobolev and Babeyko, 2005), the dilatation angle is zero, and the angle of friction is 30.6° (equivalent to a 20° angle of Coulomb material or a 0.36 coefficient of friction). For plane strain and non-dilatant flow, the Drucker-Prager friction angle β is related to the Mohr-Coulomb friction angle

102 ϕ by the equation: tan β = sin ϕ * ($3^{0.5}$). The Drucker-Prager shear yield stress or
103 cohesion is 1.63 times the Mohr-Coulomb cohesion (Abaqus user manual version 6.6).
104 The results are similar to increasing the friction of the upper plate to 30° in Mohr
105 Coulomb (friction 0.58) and the friction at the thrust interface proportionally. Interface
106 frictions of 0.4, 0.3, 0.2 and 0.1 must be changed to 0.63, 0.48, 0.32 and 0.16
107 respectively. Throughout the study, we refer to zones of high strain as faults, although
108 we do not take strain weakening into account. The backarc is fixed horizontally, and the
109 convergence along the thrust fault occurs at a rate of 91 mm/yr.
110 A natural thrust interface is generally composed of a seismogenic zone above
111 and below which stable sliding is favoured. The updip limit of the seismogenic zone is
112 usually controlled by temperatures of 100-150°C and the downdip limit corresponds to
113 either the 350°C isotherm or the Moho (Tichelaar and Ruff, 1993; Oleskevich et al.,
114 1999). Observed updip limits vary from 2-15 km, while downdip limits can vary from
115 25-50 km. Although we do not simulate the seismic cycle, we use a similar
116 segmentation of the thrust interface. Initially, we choose to divide the thrust interface
117 into three segments of equal length with transitions at 15, 30 and 45 km depth. The
118 friction of the thrust interface is varied by 0.1 from 0 to 0.4. The deepest segment,
119 below 45 km, has zero friction in all models. Our next model has modified transition
120 depths and curvature to better fit observations in Nicaragua. Our models test
121 heterogeneities restricted to the thrust interface. We later discuss how segmentation
122 affects Nicaragua.
123
124 **2b. Numerical method**
125 The finite element program used has several ways to introduce a frictional thrust
126 fault. We choose to use a surface-to-surface contact and finite sliding. We note that the

127 contact interface obeys Coulomb frictional rheology, which is equivalent to modelling a
128 subduction channel of plastic material. The friction of the contact interface μ is related
129 to the angle of friction ϕ of the channel plastic material by ϕ=ATAN(μ).

130 The elements used in Abaqus are 2D plane strain quadrilaterals with a mean size
131 of 2 km². We use the automatic meshing provided by the software with quadrilateral-
132 dominated, free and advancing front techniques to construct the initial mesh and the
133 ALE Arbitrary Lagrangian Eulerian adaptive meshing, which improves the mesh during
134 deformation. To model deformation caused only by convergence and not gravitational
135 forces, we combine two methods implemented in Wang and He (1996) and Ellis et al.
136 (2006). We first perform a run with no motion of the subducting slab and a Poisson ratio
137 of 0.5 (incompressible) (Wang and He, 1996). The gravity ramps up from zero to its
138 maximum value over 100,000 years. This allows the contact between the slab and the
139 upper plate to stabilise and to have negligible deformation of the upper plate under the
140 gravitational load, i.e. no subsidence and no sliding along the fault. The resulting
141 stresses s11, s22, s33 and s12 correspond to hydrostatic pressures ρgz, where z equals
142 depth (Fig. 3). We enter these stresses as initial conditions into a second process with a
143 Poisson ratio of 0.25 (Ellis et al., 2006). Gravity in the upper plate is entered
144 progressively in a new first step. In a second step of 200,000 years, the slab subducts.

145 In the first part, we parametrically study the effect of varying friction with depth
146 on the kinematics of deformation in the hanging wall. We then explore different models
147 to determine conditions that reproduce the kinematics of Middle Miocene forearc
148 deformation in Nicaragua.

149

150

151

3. Results of the parametric study

We present theoretical models with segments of various frictions (Figs. 3-5, Table 1). The structures obtained are a combination of two end-members: (1) a pop-up and (2) a system of antithetic faults (antithetic relative to the megathrust).

A pop-up structure represents a system with two symmetric thrust faults rooted at the same depth (Fig. 3); the seaward-oriented thrust forms first and is always dominant. The two branches of maximum strain are similar to those found in other analogue or numerical simulations (Braun and Beaumont, 1995; Beaumont et al., 1996; Buiter et al., 2006). The seaward thrust fault separates the outer forearc zone of net subsidence from the inner forearc zone of net uplift.

Pop-up structures are the most common feature in our models. Their root may be related or unrelated to segmentation of the plate interface, depending on the friction and geometry used, i.e. depth and length of the patches. The pop-up roots at the end of the frictional patch, when the friction is high (here equal to 0.4; Fig. 3 left). A short and shallow patch of 0.3 friction also leads to a pop-up structure rooted at the end of the high-friction patch (model U03M00L00, Table 1). Pop-ups may also root within the frictional patch. For lower frictions, such as 0.2 and 0.3 with a 45 km-long patch, pop-up structures propagate from a depth much shallower than the end of coupling (Fig. 3 right). Using a frictional interface down to 45 km, thrust faults arise at depths that become shallower with decreasing friction: 30 km for μ=0.4 (Fig. 4), 15 km for μ=0.3 (Fig. 3) and 4 km for μ=0.2 (Table 1), explained below.

Multiple thrust fault systems can arise when the first and deepest pop-up stops developing; this allows shallower pop-ups to form (Figs. 3, A1). The change from sticking to sliding depends not only on the shear stress along the interface but also on

177 the pressure on the fault, which is a function of friction and normal stress. The deep
178 portion of the thrust interface initially accumulates more shear stress than the shallower
179 portion and may thus slide at an early stage as e.g. in Figure 3 in the right panel. Shear
180 stress stops accumulating at the deep interface, and therefore strain above this segment
181 stops accumulating. However, increasing stress and strain at shallower levels may lead
182 to a new pop-up (Fig. A1).

183 A combination of pop-ups rooting at 30 or 40 km and a landward fault rooting at
184 45 km was produced in four cases, with high (μ=0.4) friction along the deep segment
185 and friction >= 0.2 for the upper and intermediate ones (Fig. 4, Table 1). In contrast,
186 antithetic thrust faults are obtained when the deep high-friction segment is sandwiched
187 between segments of low 0-0.2 friction (Fig. 5). The antithetic thrust faults root at the
188 updip and downdip end of the high-friction segment. Local uplift is observed in the
189 subsidence zone, and the topography at the landward and wider zone of uplift is tilted.
190 The amount of subsidence and uplift is about 2-4 mm/yr, i.e. one order of magnitude
191 lower than the values found in models with pop-up structures. Why is there localized
192 deformation parallel to the frictional interface? Why don't we have one pop-up with a
193 large root? Our interpretation follows.

194 First, when friction is high from the trench to 45 km depth, each node along
195 the thrust interface moves toward the downdip limit (Fig. 6). Since the wedge tip is free
196 to move, node displacement is about the same in the upper segments and the elements
197 are not sheared. At the downdip limit, however, node displacement must decrease to
198 zero, because the frictionless deep segment does not move with the slab. Consequently,
199 the area near the downdip limit undergoes maximum shearing. Deformation (or non-
200 deformation) of elements along the megathrust is transmitted to the upper plate. The
201 wedge tip remains relatively undeformed while the short area of high shear causes a

pop-up to form. A similar process likely occurs when a high-friction segment is sandwiched between low-friction or frictionless segments (Fig. 6). At the updip limit there must be an increase of nodal displacement. Along the high-friction patch, the maximum principal plastic strain seems to fluctuate because it does not take into account length changes (see animations in appendix). The increase of logarithmic strain or increment of strain, however, is continuous.

There are two ways to accommodate shortening by strain localisation in the upper plate: a) pushing a piece of crust upward (pop-up) or b) block rotation similar to bookshelf faulting. We suggest that the parallel fault system results from a combination of these two types of deformation, which may explain the lack of symmetry and the tilt of the basin (Fig. 1d). Block rotation may be enhanced by material redistribution from the updip limit to the downdip limit along the high-friction patch (Fig. 6). Since we do not simulate erosion and accretion, the redistribution of material can be only limited here.

We tested the effect of low intermediate friction between upper and lower segments of high friction (U04M01L04, Fig. 7); this causes a dominant pop-up rooted at the downdip end of the upper segment at 15 km depth and an antithetic fault system along the lower segment (from 30 to 45 km) similar to the previous model (U02M02L04; Figure 4, right). Finally, models with 0.2-0.3 friction below 15 km have no strain localisation, as do models with friction at the interface < 0.1, as predicted for the "pure subduction" mode described in Beaumont et al. (1999) (Table 1). No strain localisation means that the deformation remains essentially elastic. Plastic deformation starts at the surface, but there is insufficient stress at depth to form a fault; after a certain period of time, no further elastic or plastic deformation occurs in the entire upper plate. Finally, we note that increasing the mantle density to 3500 kg/m³ below 45 km depth

adds loading to the frictionless part of the thrust interface but does not affect these parametric results.

4. Comparison to Nicaraguan structures

The formation of the Sandino basin started in the late Cretaceous and may have been associated with uplift near the trench (Ranero et al., 2000). Walther et al. (2000) favour passive accumulation of sediments in deep-water behind a plateau arriving near a former trench. Local uplift in the basin and broad coastal uplift were not active at that time. During the Middle Miocene, subsidence was margin-wide and local uplift occurred in the centre of the basin during overall subsidence (Ranero et al., 2000). Here, we test a possible relationship between Middle Miocene kinematics and coupling at the subduction thrust interface. The above models with two antithetic faults (Fig. 5) are reminiscent of the structures in Nicaragua. We find that we must significantly change the location of the subduction thrust fault and slightly alter the geometry of the model to imitate the Nicaraguan deformation (i.e., slab dip and the size of the high-friction patch).

In order to reproduce the Nicaraguan faults, we use the spacing between the two thrust faults, the distance from the trench and the horizontal extent of the outer-forearc uplift zone as constraints (Fig. 8). In Nicaragua, the spacing is about 30 km, excluding the model with two segments of high friction (which produces 100 km spacing; U01M04L04). The distance from the trench to local uplift is about 120 km, removing the model with a shallow high-friction segment (which produces only 70 km; U01M04L00). Regarding the last models (U01M01L04, U02M02L04), the first uplifted zone (first strain peak) is located 30-40 km from the trench (Fig. 8a). For deeper coupled zones, the two strain peaks migrate landward. The first peak may better

252 correlate with the location of basin uplift, but the second strain peak is observed in the
253 backarc and cannot explain coastal uplift. In addition, the modelled large outer forearc
254 uplift zone cannot be reconciled with observed local uplift. Decreasing the length of the
255 high-friction segment at depth raises this zone significantly due to increasing interplay
256 between the stress fields at the updip and downdip limits of the high-friction segment.
257 Therefore, we conclude that the pattern of forearc deformation observed in Nicaragua
258 cannot be reproduced using the present geometry of the subduction zone.

259 In the late Miocene a depression formed near the arc, possibly due to increasing
260 dip of the slab (Weinberg, 1992) (Fig. 1b). We therefore test the effect of a shallower
261 dip of the subducting plate using a flat slab dipping 11° (Fig. 8b). Our results do not
262 support this interpretation, as they are similar to the above models. We can fit the
263 forearc deformation, however, by translating the subducting plate interface landward by
264 50 km, and by using a geometry of the slab that follows that of the high velocity blocks
265 (Fig. 8c). The new model reduces the distance between the first predicted peak and the
266 observed local uplift and decreases the extent of deformation in the basin, (i.e. it causes
267 more localized strain). The second predicted peak remains near the coast. No strain
268 localization occurs when we test lower friction of the middle segment equivalent to the
269 hanging-wall friction (0.36). A higher-friction patch is required to reproduce the
270 kinematics observed in Nicaragua.

271

272

273 **5. Discussion**

274 Based on seismic wide-angle measurements, Walther et al. (2000) suggested
275 subduction and accretion of a plateau followed by slab detachment and subduction
276 retreat. Below, we discuss modelling results, in particular the significance of high

277 friction and the predicted segmentation of the thrust interface, and whether our results
278 and other observations support the interpretation of Walther et al.
279
280 **High basal friction**
281 We used basic Coulomb friction at the plate interface. The rigid plate sticks to
282 the upper plate until shear stress at the interface reaches a shear stress limit that depends
283 on the normal stress and friction. Beyond this value, the slab slides at a constant shear
284 stress and no more stress accumulates. This means that in our models, plastic
285 deformation occurs at the very initiation of subduction and that high stress along the
286 thrust interface or high frictional contact is required for more shear stress to accumulate
287 prior to slip. The 0.1 Myr deformation timescale in our modelling is much lower than
288 the 10 Myr of observed deformation in Nicaragua. Moreover, the 0.4 high coefficient of
289 friction contrasts with actual values of friction thought to be as low as 0.1-0.001 based
290 on the lack of a heat flow anomaly on faults (Lachenbruch and Sass, 1980) or on
291 thermomechanical models of convergence (Sobolev and Babeyko, 2005). We therefore
292 discuss whether this discrepancy is due to processes not included in our model or
293 whether the high friction is consistent with plateau accretion and subduction retreat.
294 The arrival of a buoyant plateau, as proposed by Walther et al. (2000) (Fig. 1c),
295 may have been accompanied by a significant decrease in convergence, which would
296 allow stress accumulation over a much longer time. However, the total amount of
297 deformation would not exceed the 0.4-0.6 km of uplift and subsidence found in our
298 modelling (Fig. 8). Other mechanisms occurring at the thrust interface and surface could
299 decrease basal stresses, subsidence and uplift rates and lengthen the deformation time.
300 For example, sedimentation in the basin, which was not taken into account in our
301 models, could reduce or delay strain localisation (Fuller et al., 2006).

Our model simulates one seismic cycle of long duration, of the order of 0.1 Myr; this is due to the high friction required to obtain strain localisation. Wang and Hu (2006) simulated earthquake cycles and focused on accretionary prisms within 10 km of the trench. Thrust faults in the prism or outer wedge developed during coseismic deformation. The inner wedge (the forearc above the seismogenic zone) was found to be stable, undergoing no compressive failure at any time during the earthquake cycle. Therefore, dynamic Coulomb wedge theory with low friction cannot explain the structures found in Nicaragua.

Sobolev et al. (2006) combined subduction with rollback and 2-3 cm/yr westward drift of the South American plate. In their models, high friction >=0.1 leads to major deformation in the upper plate and slab break-off after 3 Myrs, which is plausible for Nicaragua (see discussion below). They found one zone of strain localisation and uplift 200 km from the trench, rooted at 100 km depth at the contact between the slab and the lithosphere-asthenosphere boundary of the upper plate. In Nicaragua, however, two zones of uplift are observed within 100 km of the trench in the forearc. We suggest therefore that high friction may be related to the arrival of a buoyant plateau and may have initiated strain localisation in the forearc and eventually slab detachment in Nicaragua. High shear stress at the thrust interface and a high strain rate in the upper plate may have occurred during a transient period. A long duration of deformation at a low strain rate may be driven by a component of regional stress added to the stress from subduction.

These studies show that processes at the subduction interface are more complex than expected and that various frictional conditions may operate at different depths, times and subduction setting.

Segmentation of the thrust interface

Beyond our discussion of friction, our models show that a higher stress level accumulates at 15-25 km depth, 50 km horizontally from a past trench in Nicaragua. The significance of the predicted segmentation of the thrust interface is unclear. We note a striking similarity between the estimated transition depths of the Middle Miocene subduction zone at 15 and 25 km and the currently observed structure of the subduction zone. The predicted past depth of coupling is 25 km depth, which is like the current depth of the seismogenic zone derived from aftershocks of the 1992 earthquake (Ide et al., 1993). The updip limit of the past coupling zone is estimated at 15 km depth in our models, similar to the 10 km derived from a model of a shallow fault responsible for the coseismic tsunami in 1992 (Satake, 1994). This would mean that the structures in the upper plate are influenced by heterogeneities at the thrust interface due to metamorphic reactions, as modeled in our study, rather than by the structure of the upper plate, which has changed through time (Fig. 1c).

Other evidence in favour of subduction retreat

The best fitting model implies that the initial megathrust fault was located 50 km landward of the current subduction zone during the Middle Miocene. Independent observations and studies favour subduction retreat. The current seismic quiescence of the Sandino basin and the outer-forearc seismic activity observed within 80 km of the trench supports a shift of subduction. Seaward migration of the volcanic arc seems to have also occurred in the Pliocene (Weinberg, 1992). Seismic data show a Wadati-Benioff zone down to 200 km only, consistent with recent subduction of a new slab (Burbach et al., 1984; Larrson and Mattson, 1987; Protti et al., 1993; Engdahl et al., 1998; Rogers et al., 2002). From geomorphic analysis and tomographic images, Rogers

et al. (2002) estimated that the slab broke off 9-6.7 Ma ago (in late Miocene) and the modern slab started subducting 3.8 Ma ago (in Pliocene) consistent with the observed length of the slab. Slab break-off was probably accompanied by mantle upwelling through the slab gap and uplift and formation of the more than 1000 m high plateau in Central America (Rogers et al., 2002). Slab break-off can be attributed to younging and increasing buoyancy of the incoming Cocos oceanic plate during the 19-10 Ma superfast spreading at the East Pacific rise (Wilson, 1996; Wortel and Spakman, 2000; Rogers et al., 2002). The accretion of a buoyant plateau probably facilitated slab tearing.

Complex modelling is required for more definitive results. Our modelling strategy does not allow us to model the evolution from the Miocene margin geometry to the current margin geometry since the slab is rigid and cannot deform in response to hanging wall deformation. We concentrated on reproducing the Miocene kinematics. A more complex model must also take into account material heterogeneities in the upper plate, e.g. mantle properties and the volcanic arc, sedimentation, horizontal stresses induced by collision of a plateau and the trench-parallel component of convergence that may induce transpression as suggested by Ranero et al. (2000).

6. Conclusion

We investigated the effect of various frictional characteristics on upper plate deformation. Varying the depth, length and friction of segments along the megathrust causes very different structures to arise in the upper plate, ranging from symmetric to antisymmetric thrust fault systems. The Middle to Upper Miocene structures in the Nicaraguan forearc could be explained by high stress accumulation from 15 to 25 km depth along an older subduction zone located 50 km landward of modern subduction.

This study supports the idea that an oceanic plateau accreted to the continental Chortis block during the Miocene, at which time, the slab broke off and the subduction zone jumped seaward.

Acknowledgment

This study was supported by a grant from the German national foundation "Deutsche Forschungsgemeinschaft DFG" to B.C. (CA459-1/2) and funding from GFZ Helmoltz Gesellschaft. We are very grateful to Nina Kukowski for discussions and for providing the program Abaqus. We acknowledge discussions with Stefan Sobolev and Caesar Ranero. We thank Susan Ellis, Christopher Fuller, an anonymous reviewer and the associate editor for constructive comments.

References

Beaumont, C., S. Ellis, J. Hamilton, and P. Fullsack (1996), Mechanical model for subduction-collision tectonics of Alpine-type compressional orogens, *Geology*, 24, 675–678.

Braun, J., and C. Beaumont (1995), Three-dimensional numerical experiments of strain partitioning at oblique plate boundaries: Implications for contrasting tectonic styles in the southern Coast Ranges, California, and central South Island, New Zealand, *J. Geophys. Res.*, 100(B9), 18,059–18,074.

Beaumont, C., S. Ellis, A. Pfiffner (1999), Dynamics of sediment subduction-accretion at convergent margins: Short-term modes, long-term deformation, and tectonic implications, J. Geophys. Res., 104(B8), 17573-17602.

402 Buiter, S. J. H.; Babeyko, A. Yu.; Ellis, S.; Gerya, T. V.; Kaus, B. J. P.; Kellner, A.;
403 Schreurs, G.; Yamada, Y. (2006): The numerical sandbox: comparison of model
404 results for a shortening and an extension experiment - *In: Buiter, S. J. H.; Schreurs,*
405 *G. (Eds.), Analogue and numerical Modelling of Crustal-Scale Processes*, 29-64.
406 Burbach, G., C. Frohlich, W. Pennington, and T. Matumoto (1984), Seismicity and
407 tectonics of the subducted Cocos plate, *J. Geophys. Res*., 89, 7719-7735.
408 Cailleau B., P.C. LaFemina, and T.H. Dixon (2007), Stress accumulation between
409 volcanoes: An explanation for intra-arc earthquakes in Nicaragua?, *Geophys. J. Int.*,
410 169, 1132–1138.
411 Elming, S., T. Rasmussen (1997), Results of magnetotelluric and gravimetric
412 measurements in western Nicaragua, Central America, *Geophys. J. Int.*, 128 (3),
413 647–658.
414 Engdahl, E.R., R. van der Hilst, R. Buland (1998) Global teleseismic earthquake
415 relocations with improved travel times and procedures for depth determination, *Bull.*
416 *Seismol. Soc. Am.*, 88, 722-743.
417 DeMets, C. (2001), A new estimate for Cocos-Caribbean plate motion: implications for
418 slip along the Central American volcanic arc, *Geophys. Res. Lett.*, 28, 4043-4046.
419 Ellis, S., J. Beavan, D. Eberhart-Phillips, and B. Stöckhert (2006), Simplified models of
420 the Alpine Fault seismic cycle: stress transfer in the mid-crust, *Geophys. J. Int.*, 166,
421 386-402.
422 Fukao, Y. (1979), Tsunami earthquakes and subduction processes near deep-sea
423 trenches, *J. Geophys. Res.*, 84, 2303-2314.
424 Fuller, C.W., S.D. Willett, and M.T. Brandon (2006), Formation of forearc basins and
425 their influence on subduction zone earthquakes, *Geology*, 34, p. 65–68.

426 Ide, S., Imamura, F., Yoshida, Y. & Abe, K., 1993. Source characteristics of the
427 Nicaraguan tsunami earthquake of September 2, 1992, *Geophys. Res. Lett.*, **20**(9),
428 863-866, 10.1029/93GL00683.
429 Lachenbruch, A.H., and Sass, J.H. (1980), Heat Flow and Energetics of the San Andreas
430 Fault Zone, *J. Geophys. Res*., 85, 6185-6223.
431 LaFemina, P.C., Dixon, T.H. & Strauch, W., 2002. Bookshelf faulting in Nicaragua,
432 *Geology*, **30**, 751-754.
433 Larsson T. & Mattson C. 1987. *Seismic Hazard Analysis in Nicaragua,* Royal
434 University of Technology, Stockholm.
435 McCaffrey, R., P. C. Zwick, Y. Bock, L. Prawirodirdjo, J. F. Genrich, C. W. Stevens, S.
436 S. O. Puntodewo, and C. Subarya (2000), Strain partitioning during oblique plate
437 convergence in northern Sumatra: Geodetic and seismologic constraints and
438 numerical modelling, *J. Geophys. Res.*, 105(B12), 28363-28376,
439 10.1029/1999JB900362.
440 Oleskevich, D.A., R.D. Hyndman, and K. Wang (1999), The updip and downdip limits
441 to great subduction earthquakes: thermal and structural models of Cascadia, south
442 Alaska, SW Japan and Chile, *J. Geophys. Res.,* 104, 14965–14991.
443 Park J.O., T. Tsuru, S. Kodaira, P. R. Cummins, and Y. Kaneda (2002), Splay Fault
444 Branching Along the Nankai Subduction Zone, *Science,*
445 297, 1157 – 1160.
446 Protti, M., F. Guendel, and K. McNally (1994), The geometry of the Wadati-Benioff
447 zone under southern Central America and its tectonic significance: results from a
448 high-resolution local seismographic network, *Phys. Earth Planet. Int.*, 84, 271-287.

449 Ranero, C. R., R. von Huene, E. Flueh, M. Duarte, D. Baca, K. McIntosh, A cross
450 section of the convergent Pacific margin of Nicaragua, Tectonics, 19(2), 335-357,
451 10.1029/1999TC900045, 2000.
452 Rogers R.D., H. Kárason and R.D. van der Hilst (2002), Epeirogenic uplift above a
453 detached slab in northern Central America, *Geology,* 30, 1031-1034.
454 Sobolev, S.V., and Babeyko A.Y. (2005) What drives orogeny in the Andes?, *Geology,*
455 33, 617–620.
456 Turner H. L. III, P. LaFemina, A. Saballos, G. S. Mattioli, P. E. Jansma, T. Dixon
457 (2007), Kinematics of the Nicaraguan forearc from GPS geodesy, Geophys. Res.
458 Lett., 34, L02302, doi:10.1029/2006GL027586.
459 Walther, C. H. E., E. R. Flueh, C. R. Ranero, R. von Huene, and W. Strauch (2000)
460 Crustal structure across the Pacific margin of Nicaragua: evidence for ophiolitic
461 basement and a shallow mantle sliver, *Geophys. J. Int.*, 141, 759-777.
462 Wang, K., and Y. Hu (2006), Accretionary prisms in subduction earthquake cycles: The
463 theory of dynamic Coulomb wedge, *J. Geophys. Res.*, 111, B06410,
464 doi:10.1029/2005JB004094.
465 Weinberg R.F. 1992. Neotectonic development of western Nicaragua, Tectonics, 141,
466 1010–1017.
467 Weyl, R. (1980) Geology of Central America, Borntreager, Berlin. 371pp.
468 Wilson, D. S., Fastest known spreading on the Miocene Cocos-Pacific plate boundary,
469 Geophys. Res. Lett., 23(21), 3003-3006, 10.1029/96GL02893, 1996.
470 Wortel, M.J.R., and W. Spakman (2000), Subduction and slab detachment in the
471 Mediterranean-Carpathian region, *Science*, 290, 1910-1917.
472 White, R.A. & Harlow, D.H., 1993. Destructive upper-crustal earthquakes of Central
473 America since 1900, *Seismol. Soc. Am. Bull.*, **38.**, 1115-1142.

Figure captions

Figure 1 - A) Central America where the Cocos plate converges with the Caribbean plate with an obliquity of 10° relative to the trench-normal direction. Today the forearc moves trench-parallel and northwest at 7-14 mm/yr, which may be related to oblique subduction and seems to be accommodated by shearing and NE-sinistral strike-slip faults or bookshelf faults along the volcanic arc (De Mets, 2001; Turner et al., 2007). B) Close-up of Nicaragua from above. Coastal uplift in the Middle Miocene was followed by formation of a depression. Today, active shearing characterises deformation in the volcanic arc. Data regarding deep on-shore structures were obtained by wide-angle seismic profiles, two boreholes Corvina and Argonaut Ar and land-stations (Walther et al., 2000). C) Deep onshore structures in Nicaragua (modified from Walther et al. (2000)). Blocks A and B have been interpreted as an accreted oceanic plateau and its lower crust respectively. Walther et al. suggested that block B was initially larger, reaching depths greater than 40 km, and was later partially detached and replaced by a mantle sliver. Block B may also be interpreted as serpentinized mantle (Walther et al., 2000). In the sedimentary basin, layers are as defined by Ranero et al. (2000). The white dots are the 1975-1982 hypocentres from Larsson and Mattson (1987). D) Closeup of basin sedimentary layers and Middle Miocene deformation phase from Ranero et al. (2000). There was coeval subsidence, local uplift and coastal uplift (the object of this study). We investigate whether this could be associated with coupling along the megathrust.

Figure 2 - Modelling set-up. Left: We start our model with no deformation by implementing gravitational forces as an initial stress field. The plate interface is

500 divided into three segments of various frictions with an additional frictionless
501 lowermost segment (white). U, M, L for upper, middle and lower segments.
502 Right: deformed grid after 200,000 years showing pop-up structure obtained
503 with high 0.4 friction of U and M segments and frictionless L segment (model
504 U04M04L00). The mean element size is 2 km².
505
506 **Figure 3 -** Symmetric faults or pop-up structures, left for a segment with high 0.4
507 friction from zero to 30 km depth (model U04M04L00, see Table), right for a
508 segment of 0.3 friction down to 45 km (model U03M03L03). a) Change of
509 topography after 200,000 years. b) Maximum in-plane plastic strain showing
510 two symmetric thrust faults rooting at the end of coupling. The geometry of
511 upper plate is presented undeformed. c) Relative tangential motion or slip
512 between the slab and upper plate using basic Coulomb friction model. Zero slip
513 means that the plates or portions of the plates still stick together after 200,000
514 years. The upper plate above the sticking segment accumulates strain. Maximum
515 slip is observed along the frictionless part of the fault and corresponds to the
516 accumulated downgoing motion of the slab. Intermediate values of slip means
517 that the plates or portions of plates stuck for a while but now slide past each
518 other.
519
520 **Figure 4 -** Two examples combining pop-up and antithetic faults after 200,000 years
521 (see also Table). "Antithetic" is relative to the megathrust. Left model
522 U04M04L04, right model U02M02L04.
523
524 **Figure 5 -** Antithetic faults. Left model U01M04L00, right model U01M04L04.

525

526 **Figure 6** - Deformed grids for a model with a pop-up and a model with antithetic thrust
527 faults showing the significant change of element dimensions along the high-
528 friction patch (see text for explanations).

529

530 **Figure 7** - Model with intermediate low friction within segments of high friction
531 (U04M01L04). The structures are similar to those in the previous model
532 U02M02L04 in Figure 4 right, except that a pop-up forms at shallow depth.

533

534 **Figure 8** - Comparison with Nicaragua. Dotted red lines are blocks defined by Walther
535 et al. (2000) (see corresponding Fig. 1). a) Strain localization resulting from the
536 geometry of the subduction zone observed today. The friction is 0.1 from 0 to 30
537 km, 0.4 from 30 to 45 km and zero at greater depths (model U01M01L04).
538 There are discrepancies between the modeled and observed structures. The
539 modeled seaward zone of uplift is too broad and too far from the local uplift in
540 Nicaragua. Ar is the location of a borehole giving constraints on basin
541 deformation and where local uplift is observed (Ranero et al., 2000). b) Shallow
542 dip of slab simulated by a flat slab. Frictions 0.1 and 0.4 are applied from 0 to
543 25 km and 25 to 30 km, respectively. c) A good fit with the features in
544 Nicaragua is obtained with a thrust interface on top of blocks A and B. Frictions
545 0.1 and 0.4 are applied from 0 to 15 km and 15 to 25 km, respectively. The
546 horizontal distance between the two uplifted zones is restrained to about 30 km
547 and the first uplift is kept local and about 120 km from the trench. Results are
548 consistent with the idea that regions of high velocities show the remnant of an
549 ophiolitic plateau that subducted in the Eocene and was later incorporated into

the upper plate. The thrust interface has therefore jumped seaward with time in accordance with the sense of volcanic arc migration.

Appendix

Figure A1 - Details of model U03M03L03 that has a friction of 0.3 down to 45 km depth (see also figure 3 after 200 000 years). The grey area beyond 130 km horizontal distance from trench corresponds to the frictionless segment of the thrust interface. a) Maximum in-plane plastic strain in the upper plate at three time steps, at about 3.8, 11 and 97 kyrs. Two areas of plastic strain begin at the surface and at the end of the high-friction patch at 45 km depth respectively, migrate to the wedge tip and become localised with time. b) Plastic strain on the surface at various time steps, c) Plastic strain along the thrust interface between slab and upper plate. d) State of the contact between slab and upper plate, i.e. sticking when the slip is zero or sliding when the slip becomes non-zero. e) Shear stress along the thrust interface. The shear stress is always zero in the frictionless segment. The shear stress limit is the product of the normal stress and the coefficient of friction. f) Pressure or normal stress on the thrust fault. There may be some small variations of normal stresses and thus of shear stress limit with time due to the deformation of the upper plate. There is therefore a feedback between the process in the upper plate and at the thrust interface. When the shear stress exceeds the shear stress limit, portion of the upper plate becomes uncoupled from the slab and accumulates no more strain which explains why there is no strain localization at the end of the high-frictional patch for this case. In other coupled portions, shear stress at the interface and plastic strain continues to increase which allows localisation.

8 Animations

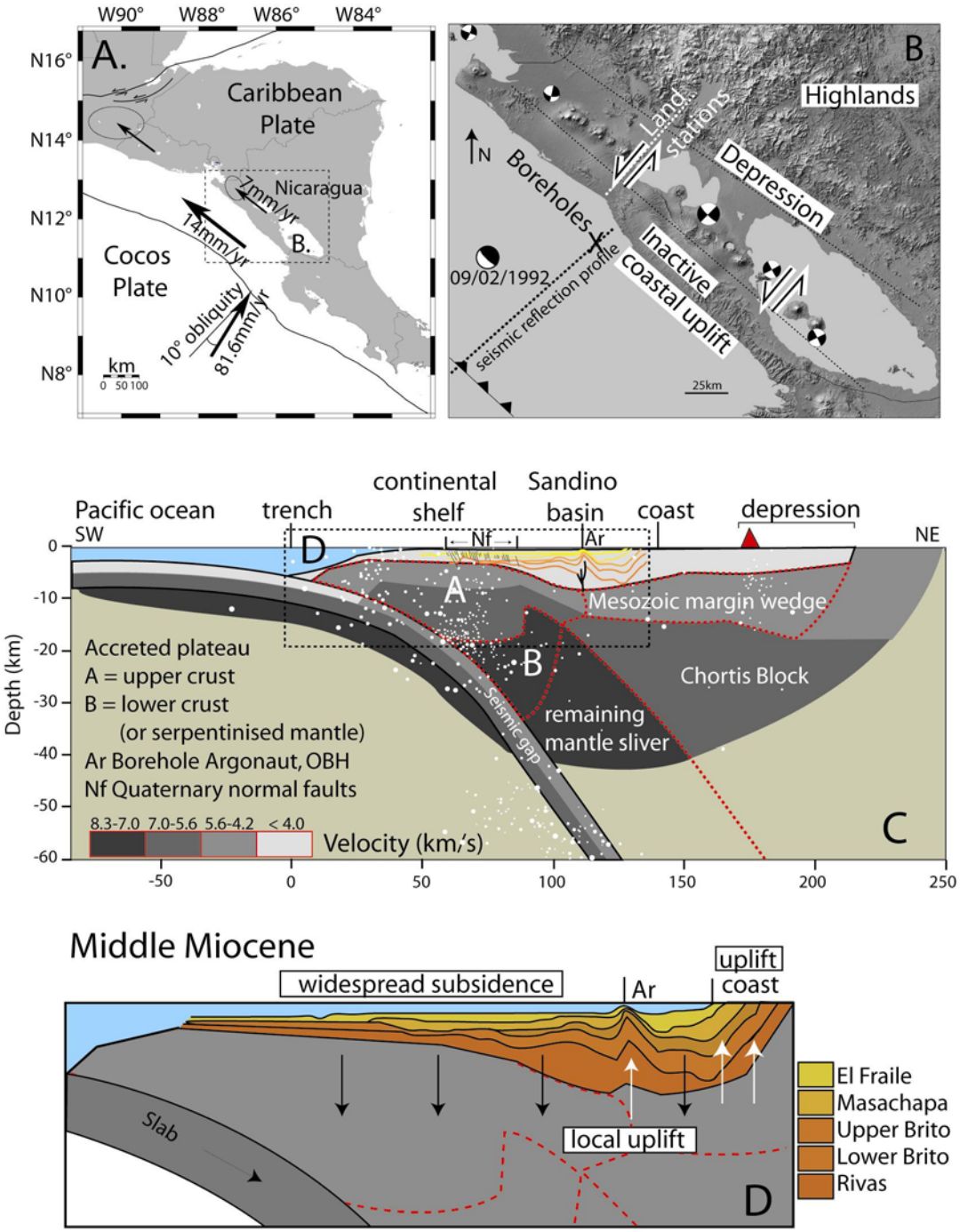

Figure 1

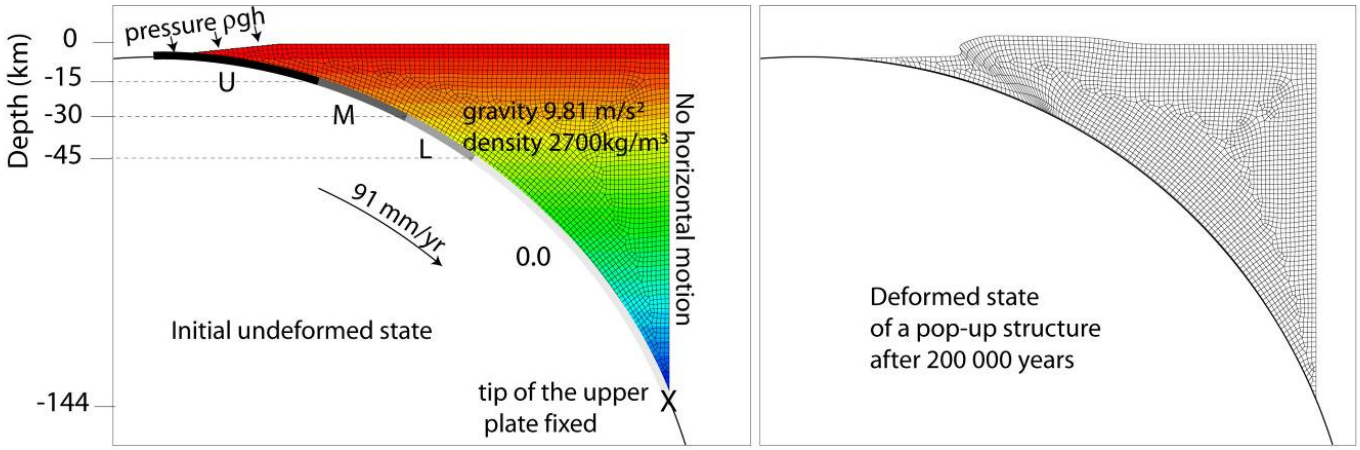
Depth (km)
0
-15
-30
-45
-144
pressure ρgh
U
M
L
gravity 9.81 m/s²
density 2700kg/m³
No horizontal motion
91 mm/yr
0.0
Initial undeformed state
tip of the upper
plate fixed
X
Deformed state
of a pop-up structure
after 200 000 years

Figure 2

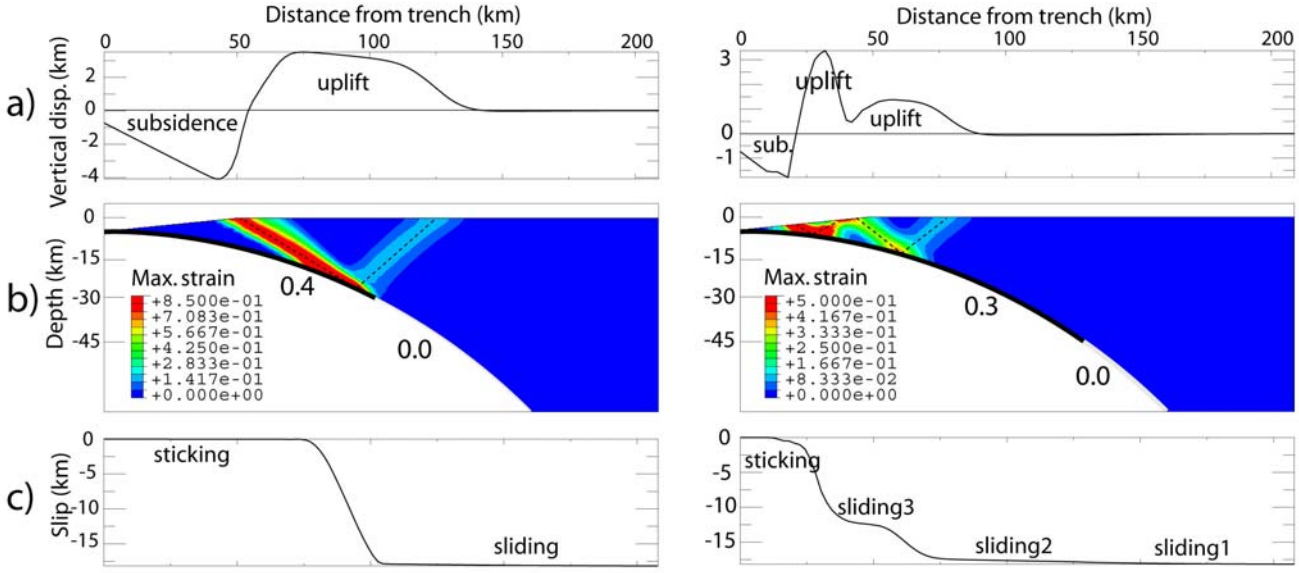

Figure 3

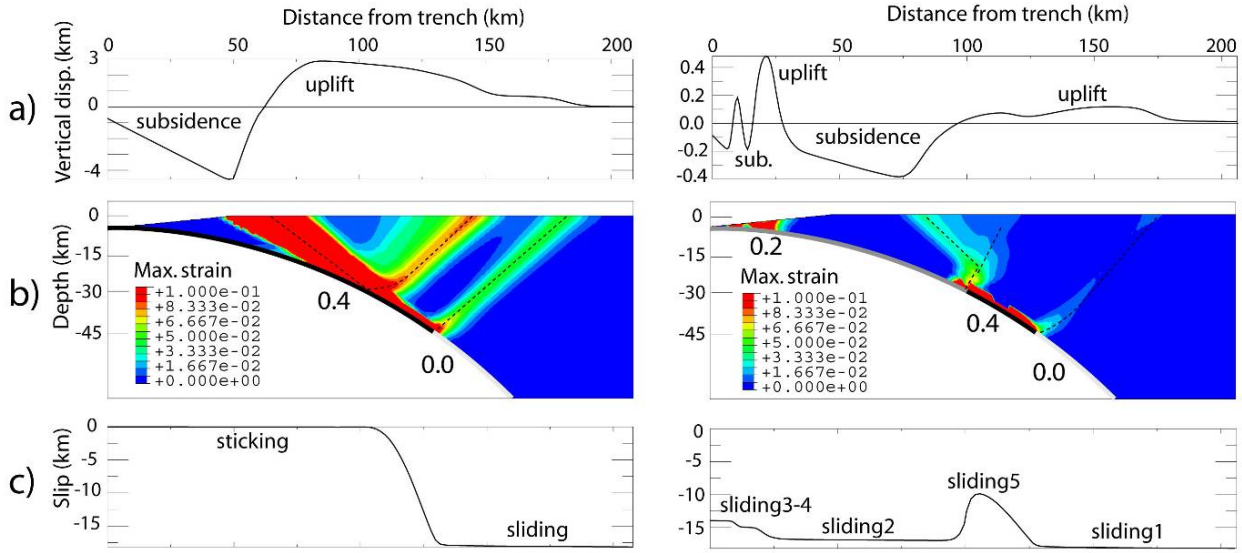

Figure 4

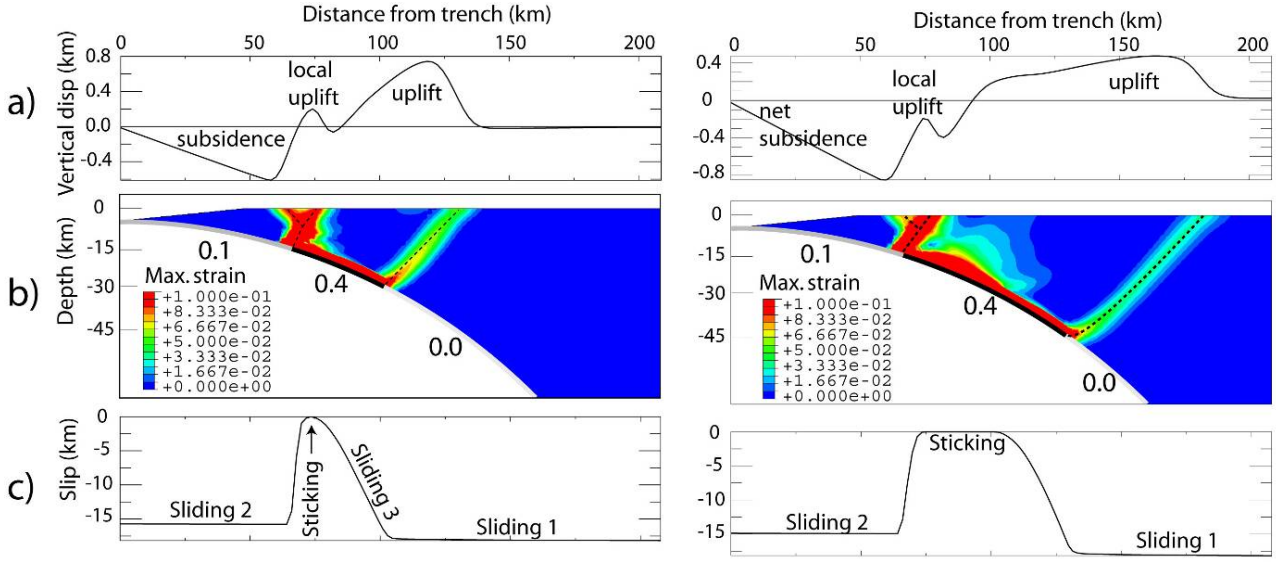

Figure 5

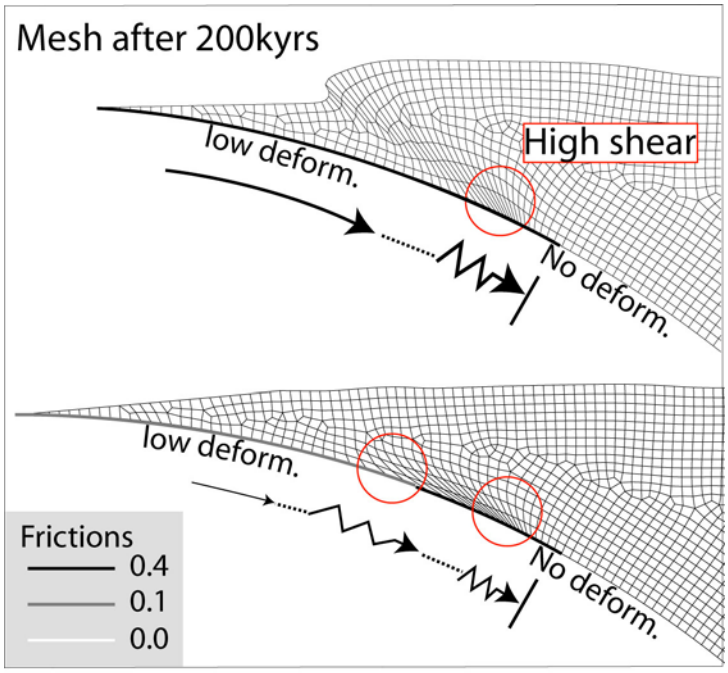

Figure 6

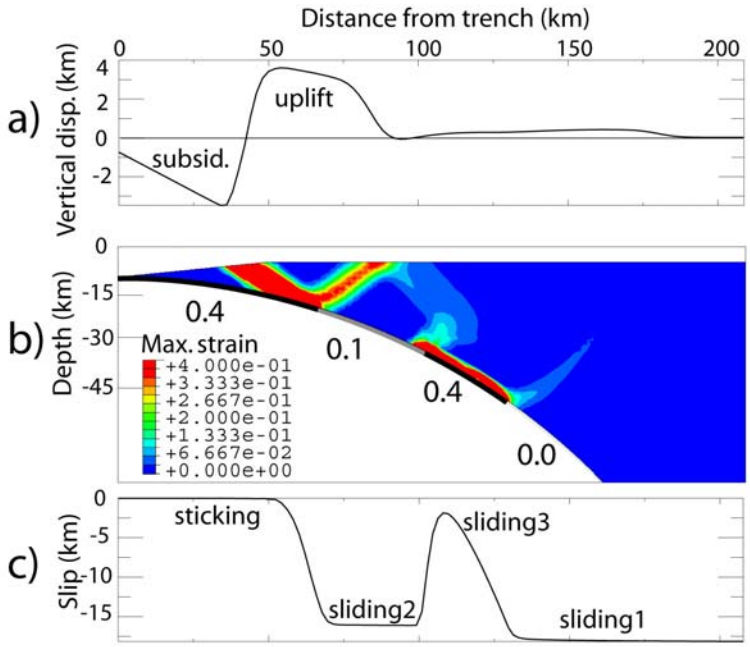
Distance from trench (km)
0
50
100
150
200
a)
Vertical disp. (km)
4
2
0
-2
uplift
subsid.
b)
Depth (km)
0
-15
-30
-45
0.4
Max. strain
+4.000e-01
+3.333e-01
+2.667e-01
+2.000e-01
+1.333e-01
+6.667e-02
+0.000e+00
0.1
0.4
0.0
c)
Slip (km)
0
-5
-10
-15
sticking
sliding2
sliding3
sliding1

Figure 7

576

577

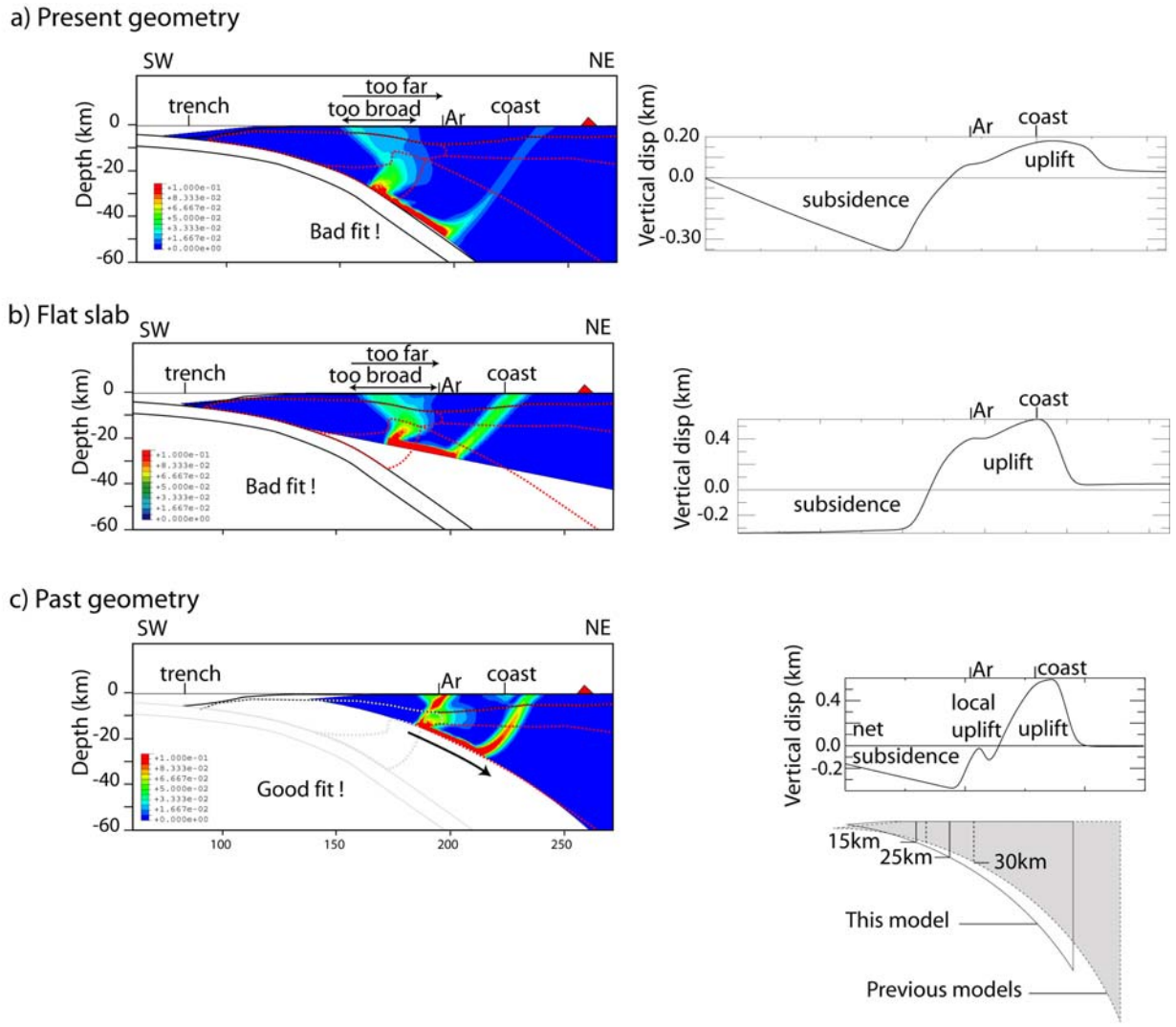
a) Present geometry
SW
NE
trench
too far
too broad
Ar
coast
Depth (km)
0
-20
-40
-60
Bad fit !
Vertical disp (km)
0.20
0.0
-0.30
subsidence
uplift
b) Flat slab
Good fit !
0.4
-0.2
c) Past geometry
100
150
200
250
local
net
15km
25km
30km
This model
Previous models

Figure 8

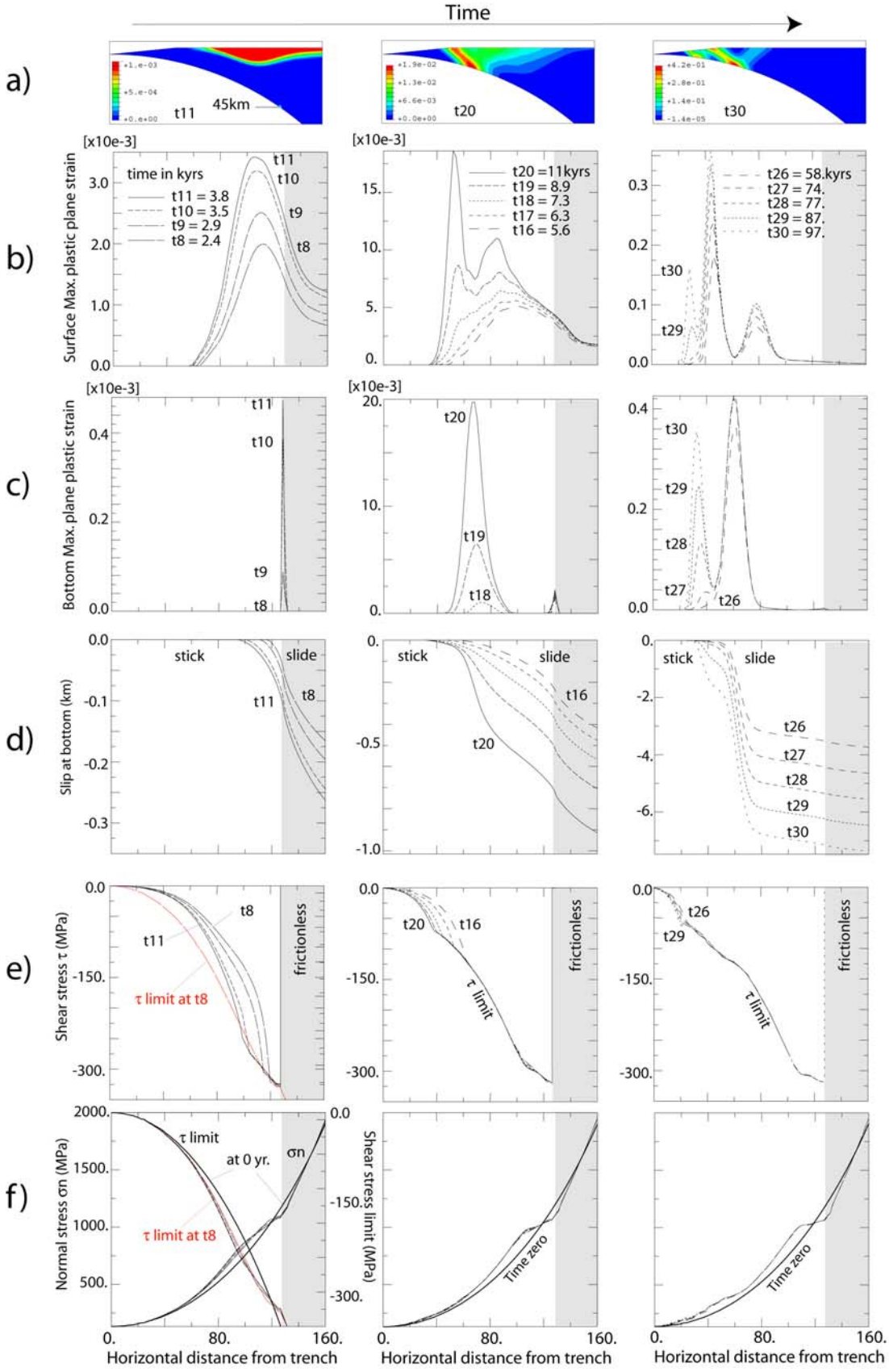
Time
a)
t11
45km
t20
t30
b)
[x10e-3]
Surface Max. plastic plane strain
time in kyrs
t11 = 3.8
t10 = 3.5
t9 = 2.9
t8 = 2.4
t20 =11kyrs
t19 = 8.9
t18 = 7.3
t17 = 6.3
t16 = 5.6
t26 = 58.kyrs
t27 = 74.
t28 = 77.
t29 = 87.
t30 = 97.
c)
Bottom Max. plane plastic strain
d)
Slip at bottom (km)
stick
slide
e)
Shear stress τ (MPa)
frictionless
τ limit at t8
τ limit
f)
Normal stress σn (MPa)
τ limit at 0 yr.
σn
Shear stress limit (MPa)
Time zero
Horizontal distance from trench

Figure A1

579

Transition depths	Frictions	Structures
Two segments		
15km	U04M00L00	Pop-up roots at 15 km
	U03M00L00	Pop-up roots at 15 km, at 5 km
	U02M00L00	Pop-up roots at 4 km
	U01M00L00	No localisation
30km	U04M04L00	Pop-up roots at 30 km
	U03M03L00	Pop-up roots at 15 km, at 5 km
	U02M02L00	Pop-up roots at 4 km
	U01M01L00	No localisation
45km	U04M04L04	Pop-up at 40 km, landward thrust at 45 km
	U03M03L03	Pop-up roots at 15 km, at 5 km
	U02M02L02	Pop-up roots at 4 km
	U01M01L01	No localisation
Three segments		
15-30km	U04M03L0 U04M02L0 U04M01L0	Pop-up at 15 km
	U03M04L0	Pop-up at 30 km, at 5 km
	U03M02L0 U03M01L0	Pop-up at 15 km, at 5 km
	U02M04L0	Pop-up at 30 km, at 4 km
	U02M03L0 U02M01L0	Pop-up at 4 km
	U01M04L0	Landward thrust to pop-up at 15 km and landward thrust at 30 km
	U01M03L0 U01M02L0	No localisation
15-45km	U04M03L03 U04M02L02 U04M01L01	Pop-up at 15 km
	U03M04L04	Pop-up at 40 km, landward thrust at 45 km
	U03M02L02 U03M01L01	Pop-up at 15 km, pop-up at 5 km
	U02M04L04	Pop-up at 40 km, landward thrust at 45 km, pop-up at 2 km
	U02M03L03 U02M01L01	Pop-up at 5 km
	U01M04L04	Landward thrusts at 15 km and 45 km, diffuse strain along segment
	U01M03L03 U01M02L02	No localisation
30-45km	U04M04L03 U04M04L02 U04M04L01	Pop-up at 30 km depth
	U03M03L04	Pop-up at 30 km and 13 km, landward thrust at 45 km
	U03M03L02 U03M03L01	Pop-up at 13 km, at 5 km
	U02M02L04	Pop-up at 5 km and 2 km, landward to seaward thrust at 30 km, and landward thrust at 45 km

	U02M02L03 U02M02L01	Pop-up at 5 km
	U01M01L04	Landward to seaward thrust at 30 and landward thrust at 45 km
	U01M01L03 U01M01L02	No localisation

Table 1 - Structures arising from various frictions at two or three segments after 200 000 years. The 1st column indicates the transition depths at which there are changes of friction. The 2nd column gives the names of the models and the frictions at each segment: U Upper segment 0-15 km, M Middle segment 15-30 km, L Lower segment 30-45 km. The deepest segment from 45 km to 150 km depth is always frictionless. All numbers in the last column are the depths from which faults or systems of faults propagate. White lines represent typical pop-up structures. Yellow lines are for resulting antithetic thrust faults relative to the megathrust fault. Blue lines are a combination of pop-up and antithetic fault. Green lines show models without strain localisation. In a pop-up, the seaward-oriented thrust forms first and is always the dominant fault compared to the landward-oriented thrust fault.